J Water Environ Nanotechnol 2026, 11(4): 522-534

10.22090/jwent.2026.2083327.2052

RESEARCH PAPER

Phyto-Hydrothermal Fabrication of ZnONPs Using *Sesuvium Portulacastrum L.* (Aizoaceae) Extract and Their Eco-Friendly Applications

Mawlood Maajal Ali[1], Hadeel Salih Mahdi[2], Rafaa Abd Alkareem Abdulwahid[1], Mustafa Nadhim Owaid[3],[4]

[1]Department of Medical Physics, College of Applied Sciences-Hit, Heet, University of Anbar, Anbar, 31007, Iraq
[2]Department of Science, College of Basic Education, University of Misan, Misan, Iraq
[3]Department of Heet Education, General Directorate of Education in Anbar, Ministry of Education, Hit, Anbar, Iraq
[4]Department of Environment, College of Applied Sciences-Hit, Heet, University of Anbar, Anbar, 31007, Iraq

*Corresponding Author. Email: mustafanowaid@gmail.com

Article History:

Received: 2026-01-07

Revised: 2026-02-27

Accepted: 2026-04-18

How to cite this article
Ali M M, Mahdi H S, Abdulwahid R A A, Owaid M N. Phyto-Hydrothermal Fabrication of ZnONPs Using Sesuvium portulacastrum L. (Aizoaceae) Extract and Their Eco-Friendly Applications. J Water Environ Nanotechnol 2026, 11(4): 522-534, DOI: 10.22090/jwent.2026.2083327.2052

HIGHLIGHTS

- Green phyto-synthesis combined with hydrothermal treatment produced ZnO NPs with higher crystallinity.
- The treated ZnO showed band-gap narrowing and defect engineering that enhanced photocatalytic and gas-sensing performance.
- T-ZnO achieved 86% dye degradation and lower gas detection limits, making it promising for environmental applications.

ABSTRACT

ZnO NPs were phytosynthezied based on ***Sesuvium portulacastrum*** L. leaf extract and modified by hydrothermal treatment to give T-ZnO NPs. A small blue shift and narrowing of the band gap were observed to be 2.86 eV (ZnO) and 2.75 eV (T-ZnO) by optical analysis, which confirmed improvement of defect formation and crystallinity. XRD and SEM confirmed that the nanoparticles were restructured and growth of nanoparticles was controlled, and that the treated nanoparticles have compacted morphologies and increased surface active sites. The contribution of the above phytochemicals in reduction and stabilization was confirmed by Fourier Transform Infrared (FTIR) spectra, while removal of organic species that had survived after the synthesis by thermal treatment assisted in bettering the quality of ZnO NPs. A higher magnitude of net surface charge, 46 mV for T-ZnO NPs as compared to 38 mV for ZnO NPs, was indicated by zeta potential analysis, confirming higher colloidal stability for T-ZnO NPs. Higher thermally labile organic content in T-ZnO, TGA confirmed successful hydrothermal surface functionalization. T-ZnO NPs also showed better photocatalytic degradation performance of 86% in 120 min with increased kinetic constants, better gas sensing response toward NH_3 (46.7%) and VOCs (50.0%), and improved detection limits of 0.4 ppm for H_2 and VOCs. These findings show that hydrothermal engineering of plant-mediated synthesis is a scalable approach to design ZnO nanostructures with enhanced optoelectronic, photocatalytic, and sensing properties for use in environmental applications.

KEYWORDS: *Green Synthesis, Hydrothermal Treatment, Photocatalytic Degradation, Gas Sensing*

©2026 The Author(s). Published by the Iranian Environmental Mutagen Society. This work is licensed under the Creative Commons Attribution 4.0 International License (CC BY 4.0). To view a copy of this license, visit http://creativecommons.org/licenses/by/4.0/.

INTRODUCTION

Due to reasonably unique properties including its large band gap, high electron mobility, and easily tunable surface chemistry, zinc oxide (ZnO) nanoparticles have shown great potential for photocatalytic, gas sensing, electronic, and environmental remediation applications. Synthesis of ZnO NPs also falls under classical approaches, which mostly involve toxic chemicals and require much energy, which create a safety and environmental risks [1]. Green synthesis using plant extracts can provide an environmentally friendly solution, in which naturally occurring biomolecules serve as reducing and capping agents, controlling the growth of nanoparticles, inducing surface defects, and enhancing functional properties [2] [3]. While work is abundant on various plant-mediated syntheses, the utility of the halophyte *Sesuvium Portulacastrum* L., rich in polyphenols and flavonoids, for ZnO nanoparticles has not been extensively explored.

Several studies have demonstrated the synthesis of ZnO nanoparticles using plant extracts. These ZnO nanoparticles have high antimicrobial activity and show remarkable results for catalytic applications. Also, the synthesized ZnO nanoparticles from seeds of *Portulaca oleracea* showed good antimicrobial activity too [4], along with antibacterial activity found in ZnO nanoparticles synthesized from *Moringa* oleifera leaves [5].

Hydrothermal treatment has also been applied to enhance the synthesis of ZnO NPs. Hossain et al. [6] indicated that compared with commercial ZnO powder, hydrothermally synthesized ZnO nanorods are more effective for the degradation of organic pollutants, which can be explained by the enhanced crystallinity and surface area. Such results confirmed that the photocatalytic effectiveness of hydrothermally synthesized ZnO/bentonite nanocomposites had been improved [7]. In addition, it was found that the physical defects induced by doping or post-synthesis treatment could benefit the gas sensing properties of the metal oxide materials. Such efforts were achieved through the enhancement of oxygen adsorption and charge transfer [8].

The combination of green synthesis and hydrothermal treatment is a synergistic strategy to tune both ON functional properties and structure states of ZnO NPs. For example, the synthesized ZnO NPs using *Azadirachta indica* (Neem) extract exhibited enhanced efficiency of dye degradation. This role helped in defect engineering and the incorporation of plant-derived elements [9] [10] [11]. Nevertheless, the potential of bio-inspired, defect-rich nanomaterials for high-performance gas sensing remained an emerging and highly promising line of research.

Photons whose energy exceeds their bandgap (Eg) are absorbed by ZnO and T-ZnO nanoparticles; electrons (e−) from the VB are excited to the CB in this process, and holes (h+) are left in the VB. Electron–hole pairs created by the process initiate redox reactions at the catalyst surface. The electrons generated by light illumination subsequently react with the adsorbed oxygen molecules, resulting in the formation of O2 ·−, and the holes oxidize water molecules or surface hydroxyl groups to yield •OH. These extremely active reactive oxygen species (ROS) are responsible for the oxidative degradation of organic pollutants into lower-molecular-weight, less toxic intermediates, and finally mineralizing into CO_2 and H_2O [9]. The primary sensing mechanism followed by ZnO and T-ZnO nanoparticles is surface adsorption coupled with charge transfer phenomena. Under ambient conditions, oxygen molecules adsorb onto the nanoparticle surface and accept free electrons from the conduction band to produce negatively charged oxygen species (O_2^-, O^-) that create a depletion layer at the surface and raise electrical resistance [10].

ZnO nanoparticles are important for their wide band gap, high chemical stability, and tunable nanostructures, which enable the generation of reactive oxygen species (ROS) for efficient degradation of organic pollutants under UV (or solar) light [11], and surface oxygen species-assisted adsorption–desorption modulates charge carriers for chemiresistive gas sensing [12]. Defect engineering, controlled morphology, and hybrid synthesis enhance charge separation, create abundant surface active sites, and increase the sensitivity by the enhancement in the selectivity towards target gas. Thus, this work anticipates an enhancement in photocatalytic degradation activity as well as an improvement in gas-sensing performance of T-ZnO NPs over conventional ZnO nanoparticles due to the structural–surface modifications achieved.

In this study, *Sesuvium Portulacastrum* L. leaf extract was employed for the green hydrothermal synthesis of ZnO NPs (T-ZnO NPs). Novel to this work is the combination of this plant approach with subsequent hydrothermal treatment, yielding a hybrid treatment that dramatically improves crystallinity, decreases the defect density, and gives controlled particle morphology. It is hypothesized that bioactive compounds of the plant act as reducing, capping, and doping agents. These features relate to changes in the morphology, crystallinity, and surface defect states. The study examined the structural and optical characteristics of the programmed ZnO NPs, which were used for photocatalytic degradation and chemiresistive gas sensing. The crux of the hypothesis is that hydrothermal treatment creates a defective surface which is beneficial for catalytic reactions and analyte adsorption. This study offers a new sustainable, simple, and scalable route to phytosynthesize multifunctional ZnO NPs using local green plant extracts. Lastly, this is the pioneering report to employ the use *Sesuvium Portulacastrum* L. in the biosynthesis of ZnO NPs and investigation towards gas-sensing applications.

MATERIALS AND METHODS

Chemicals

Zinc nitrate hexahydrate [$Zn(NO_3)_2{\cdot}6H_2O$] was used as the zinc precursor for the synthesis of ZnO nanoparticles. Fresh leaves of *Sesuvium portulacastrum* L. were collected and washed with distilled water. The collected leaves were processed in the laboratory and used as both a reducing and capping agent in the synthesis process. Methylene blue (Sigma-Aldrich) and double-distilled water (DDW) were utilized in all synthesis procedures to ensure a high purity grade of solvents. All reagents were used as received from manufacturers, without any further purification.

Synthesis of ZnO Nanoparticles (ZnO NPs)

Green synthesis of Zinc Oxide nanoparticles was carried out following the method reported by Mahajan, Munisha et al. [13]. Briefly, approximately 3g of zinc nitrate hexahydrate was dissolved in 100 mL of DDW and constantly stirred at 600 rpm using a magnetic stirrer. 30 mL of *Sesuvium portulacastrum* leaf extract was added dropwise to the precursor solution. This led to the formation of a homogeneous colloidal suspension, indicating nanoparticle formation. The suspension was transferred into Petri dishes and was oven-dried at 65-70 °C for 6 hr. After drying, the residue was calcined in a porcelain crucible at 350 °C for 4 hr to enhance crystallinity. The synthesized ZnO powder was ground to a fine powder using an agate mortar and pestle and stored in sterile Eppendorf tubes for further characterization and application.

Synthesis of Hydrothermally Treated ZnO Nanoparticles (T-ZnO NPs)

For the hydrothermal treatment, the colloidal reactants composed of zinc nitrate and a plant extract were taken and placed in a Teflon-lined stainless-steel autoclave and held at a temperature of 170 °C for a duration of 5 hr in a hot-air oven, following the method reported by Ali et al. [14]. After cooling the solution of NPs, it was placed in an oven at 65°C for 6 hr to dry, and then calcined at 350°C for 4 hr to calcine the sample before use in the investigations. The collected product was finely ground with an agate mortar and stored in sterile Eppendorf tubes for physicochemical characterization and photocatalytic analysis.

Preparation of ZnONPs and T-ZnONPs Electrodes

Commercial interdigitated electrodes (IDEs) on glass support were used to create the films. For gas sensing measurements, ZnO and T-ZnO nanoparticles were dispersed in a solution of ethanol and a small amount of ethyl cellulose binder and sonicated for 10–20 min to ensure a homogeneous suspension. The suspension was then uniformly deposited onto the IDEs by drop-casting and dried at 80-100°C to remove the solvent. The coated electrodes were finally annealed at 350 °C for 2 h to increase crystallinity and remove organic binders, creating a reproducible and active sensing layer.

Characterization of the synthesized NPs

The ZnO obtained in the laboratory and the hydrothermally treated ZnO were completely characterized to demonstrate their structural, optical, and morphological properties. Observations of the samples' optical properties were made using a UV–visible spectrophotometer (Shimadzu UV-1900, Japan) with the range of 190–800 nm. Spectra were collected using double distilled water as a reference, a resolution of 1 nm, and a scanning rate of 200 nm·min^{-1}, in a quartz cuvette with a 1 cm path length.

The crystal structure was examined via X-ray diffraction (XRD, Phillips) using Cu Kα radiation (λ = 1.5406 Å). Diffraction patterns were collected over the 2θ range of 10°–80° to determine crystallite size and phase makeup. Surface morphology was assessed using field-emission scanning electron microscopy (SEM, Tescan Mira3, France) operating with an accelerating voltage of 15 kV for particle shape and surface texture analysis. The plant extract and the resultant nanoparticles were analysed with Fourier Transform Infrared Spectroscopy (FTIR 7800A, UK) over a wavenumber range of 4000–400 cm^{-1}. Zeta potential measurements were done using a Malvern ZS (UK) to evaluate the colloidal stability. Thermogravimetric analysis (TGA) is a common method that is employed in thermal studies for measuring changes in the mass of materials when the materials are subject to heat from -20 to 900°C in the presence of nitrogen at a scan rate of 10°C/min (Perkin-Elmer 4000).

Photocatalytic Activity

The photocatalytic performance of ZnO and hydrothermally treated ZnO (T-ZnO) nanoparticles was studied using a UV lamp (365 nm) as the irradiation source. Methylene blue (MB, 10 ppm) was selected as a model organic pollutant for each experiment. All tests were done in a dark chamber to prevent light interference, and the degradation efficacy was examined with different experimental conditions, including irradiation time, pH, temperature, and initial concentration of MB. Each experiment was replicated three times.

The degradation efficacy (%) of MB was determined using Eq. (1):

$$Degradation(\%) = \frac{A_o - A_t}{A_o} x100 \quad (1)$$

where A_o is the initial absorbance of MB and A_t is the absorbance after irradiation at time t [15].

The photocatalytic kinetics were further analyzed using a pseudo-first-order model (Eq. 2):

$$\ln(\frac{C_o}{C_t}) = k.t \quad (2)$$

J Water Environ Nanotechnol, 2026, 11(4): 522-534
10.22090/jwent.2026.2083327.2052

where C_0 and C_t are the MB concentrations at the beginning and at irradiation time t, respectively, and k is the apparent rate constant (min^{-1}) [16].

Sensor Response

The sensor response (S) was calculated using the formula Eq. (3):

$$S = \frac{R_{air} - R_{gas}}{R_{air}} x100\% \quad (3)$$

where R_{air} is the baseline resistance in air, and R_{gas} is the resistance in the target gas. A higher response indicates a greater change in resistance upon exposure to the gas, reflecting the sensor's sensitivity [17]. Additionally, the detection limit (DL) was estimated using the formula Eq. (4):

$$DL = \frac{3xSD}{Slope} \quad (4)$$

where SD is the standard deviation of the baseline resistance, and Slope is the rate of change of resistance with respect to gas concentration. This formula helps determine the lowest concentration of gas that can be reliably detected by the sensor [18].

RESULTS AND DISCUSSION:

The UV-Vis absorption spectra (Fig. 1) demonstrate that hydrothermally treated, plant-extract-mediated ZnO nanoparticles (T-ZnO NPs), synthesized through a method different from their conventional analogues (ZnO NPs), exhibit optical enhancement characteristics. Although both samples exhibited a peak at approximately 371 nm, T-ZnO NPs showed a slight blue shift to 368 nm, which indicates a decrease in particle size and increase in crystallinity of T-ZnO NPs.The lack of any significant broad background absorption in T-ZnO NPs (compared to the pure plant extract) confirms substantial removal of organic residues as possible charge recombination centres. These enhancements suggest that T-ZnO NPs produced via the green–hydrothermal method are highly promising for photocatalytic and optoelectronic applications, where minimising defects is essential [19][20].

A clear and characteristic absorption peak of ZnO NPs is observed at λmax 371 nm. This peak confirms the successful formation of ZnO NPs and corresponds to the excitonic absorption / band-edge transition of these nanoparticles. The relatively higher absorbance intensity (Abs = 0.859) may be associated with smaller particle size[21], surface defects, or residual plant-derived capping agents on the nanoparticle surface [22][23]. However, the absorption peak shifts slightly to 368 nm, showing a blue shift compared to untreated ZnO NPs. This blue shift indicates improved crystallinity [24], partial removal of organic residues after thermal treatment (leading to a decrease in intensity), and modification of the electronic structure of ZnO. Reduced defect density and removal of organic residues (0.419) suggest reduced defect density and enhanced structural ordering due to thermal treatment [25].

Overall, the lower absorbance of thermally-treated ZnO NPs compared to untreated ones is dominantly ascribed to the decomposition of residual organic capping agents, higher crystallinity, fewer defects, and grain growth during thermal treatment. These effects combined cause less light to scatter and be absorbed, resulting in a reduced absorbance overall intensity. Thermal treatment encourages particle sintering; however, Scherrer analysis reveals a small decrease in crystallite size that is associated with the rearrangement of defects and points to an increased disorder in thermally prepared samples. As a result, the surface-to-volume ratio decreases, reducing the number

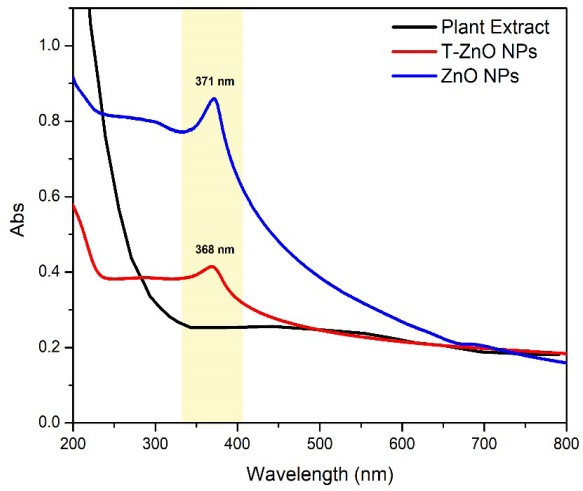


Fig. 1: UV–Vis absorption spectra of plant extract, ZnO NPs, and T-ZnO NPs.

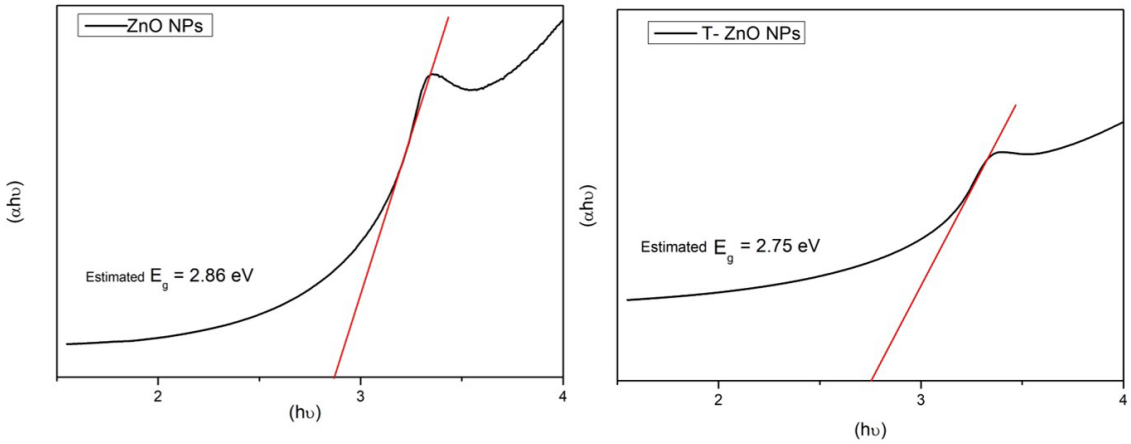


Fig. 2: Tauc plots showing band gap reduction from 2.86 eV (ZnO NPs) to 2.75 eV (T-ZnO NPs).

of surface-active sites that contribute to light absorption, and consequently lowering the overall absorbance intensity [26]. Thermally treated ZnO nanoparticles exhibit more uniform size and improved structural regularity, which reduces light scattering effects. In contrast, untreated nanoparticles with smaller sizes and irregular shapes cause higher scattering [27], which is recorded as apparent absorbance. Consequently, thermal treatment leads to lower measured absorbance intensity.

The UV–Vis absorption spectra and corresponding Tauc plot analysis (Fig. 2) reveal a notable improvement in the electronic properties of hydrothermally treated, plant-extract-synthesized ZnO nanoparticles (T-ZnO NPs) compared to conventionally synthesized ZnO NPs. The Tauc plot indicates a reduction in the direct band gap of T-ZnO NPs to 2.75 eV, compared with 2.86 eV for standard ZnO NPs. This band gap narrowing suggests the introduction of defect states or bio-organic doping within the ZnO lattice, facilitated by the plant-extract capping agents incorporated during hydrothermal treatment [28]. Additionally, the sharper absorption edge and more linear Tauc plot region for T-ZnO NPs indicate higher crystallinity and fewer disordered domains that typically contribute to tailing states. Such an optimized electronic structure, with a narrower but well-defined band gap, enhances light absorption while maintaining efficient charge carrier separation, making T-ZnO NPs highly promising for photocatalytic and photovoltaic applications [29].

The optical band gaps of the ZnO and T-ZnO NPs were estimated using the Tauc plot method, based on the relation (Eq. 5):

$$(\alpha h\nu)^n = A(h\nu - Eg) \quad (5)$$

Where α is the absorption coefficient, hν is the photon energy, A is a proportionality constant, and n=2 for direct allowed transitions [30].

The images of Scanning Electron Microscopy (SEM) and the particle size distribution showed that T-ZnO NPs have a relatively smaller size with a more regular monodisperse form rather than the conventional ZnO NPs. The size distribution was well fitted with the Gaussian (controlled particle size), which is required to mitigate the defect-mediated charge recombination. The optimal morphology of green-hydrothermal ZnONPs provided a larger effective surface area and facilitated charge carrier dynamics. This narrower band gap and better morphology highlight the increased photocatalytic and optoelectronic capabilities of T-ZnO NPs compared to traditional ZnO NPs [31] [32].

The image of SEM (Fig. 3a) showed irregularly shaped and loosely aggregated zinc oxide nanoparticles in small clusters with less-defined boundaries. The surface morphology is relatively rough and highly agglomerated. This result indicated incomplete crystal growth or less uniform nucleation. The histogram of ZnONPs (Fig. 3a) showed a broad distribution, ranging roughly from 20nm to 90 nm, with most particles centered around 45-55 nm. Whereas Fig. 3b (the SEM after the hydrothermal treatment) showed more developed, well-defined, and compact nanostructures. The aggregation of NPs is still present but appears more organized and denser, which improves the nature of crystals. The final shape indicated partial growth and restructuring during the thermal-hydrothermal process. Moreover, the histogram in Fig. 3b showed a distribution mainly in the 50-70 nm range, with some larger outliers. The growth of several larger zinc oxide NPs (approx. 114 nm) indicated crystal coalescence and size maturation due to the hydrothermal heating [33]. Size-related improvement was clear during the slight increase in average size of NPs. Indication of crystal growth and improved crystallinity and distribution becomes more controlled, although larger aggregates appear.

Energy-Dispersive X-ray (EDX) spectroscopy (Fig. 3, c&d)

J Water Environ Nanotechnol, 2026, 11(4): 522-534
10.22090/jwent.2026.2083327.2052

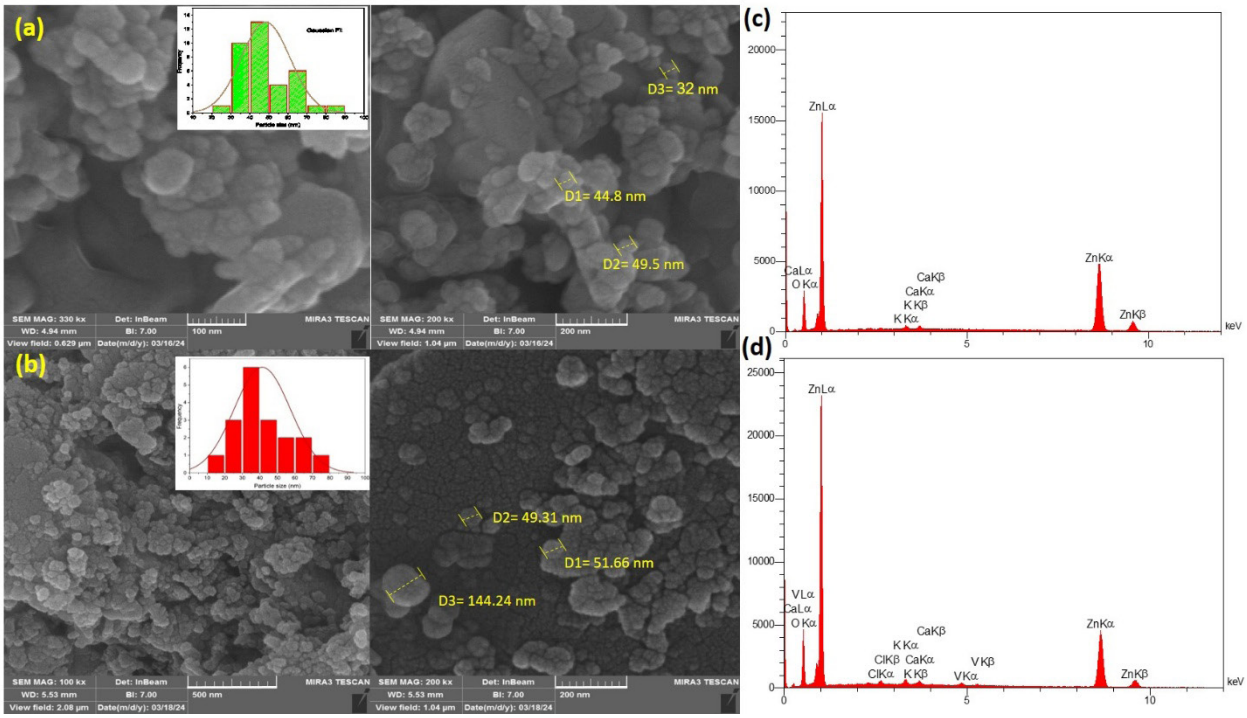


Fig. 3: SEM images of **(a)** ZnO NPs and **(b)** T-ZnO NPs and EDX spectra of **(c)** ZnO NPs & **(d)** T-ZnO NPs showing incorporation of C, K, and Ca.

revealed the presence of carbon (C), potassium (K), and calcium (Ca) peaks in the T-ZnO NP spectrum. These results indicate that the incorporation of plant elements into the ZnO matrix was successful. The doping of the ZnO structure with elemental species (like carbon) is known to introduce intra-bandgap energy states that narrow the band gap and improve light absorption. Also, SEM demonstrated that bio-functionalization promoted a more monodisperse and uniform morphology, as organic constituents from the plant extract act as natural capping agents during hydrothermal synthesis. This control over nucleation and growth minimizes agglomeration and defect formation, which is critical for effective charge carrier separation [34]. Collectively, the synergistic combination of elemental doping and morphology control inherent to this green–hydrothermal route produces an advanced photocatalyst with superior visible-light activity. The presence of Ca and K signals in the EDX spectrum of ZnO nanoparticles can be attributed to mineral constituents naturally present in the plant extract used during green synthesis, which may remain adsorbed on the nanoparticle surface as residual impurities or stabilizing species[25] [22]. Oxygen originates from the ZnO lattice and surface hydroxyl groups, as commonly reported for biogenically synthesized ZnO NPs [21].

X-ray Diffraction (XRD) patterns (Fig. 4) verify the successful preparation of ZnO nanoparticles. All accessible diffraction peaks are indexed to the characteristic planes attributed to ZnO with no signs of contaminants in the NPs.

Good crystals of T-ZnO NPs (the ZnO synthesized by the hydrothermal method). In comparison with the normal ZnO NPs, this sample has sharper and more intense diffraction peaks. This was evident by the narrowing of the peaks at (101) and (100) planes, which indicated the enhancement of crystallinity. On the other hand, the Scherrer analysis indicated that T-ZnO NPs had a somewhat lower crystallite size compared to the T0-ZnO NPs despite an overall improved crystallinity. The improved crystallinity of the T-ZnO resulted in superior electron transport properties thereof, which can be helpful in applications where the mobility of charge carriers needs to be enhanced, such as photocatalysis or nanoelectronics [35] [36]. The overall nanoparticle size may increase while the crystallite size decreases due to the grain coalescence.

The functional groups in the extract of the plant (*Sesuvium portulacastrum* L.), which are involved in the reduction and stabilization of zinc oxide nanoparticles, were characterized using FTIR spectroscopy. FTIR spectra of the plant extract sample, ZnO NPs, and T-ZnO NPs are presented in Fig. 5. A representative spectrum for the plant extract displayed broad and intense absorption bands in the O-H stretching region spanning from 3200 cm^{-1} to 3600 cm^{-1}, indicating the presence of phenolic compounds and alcohols [37]. The bands observed

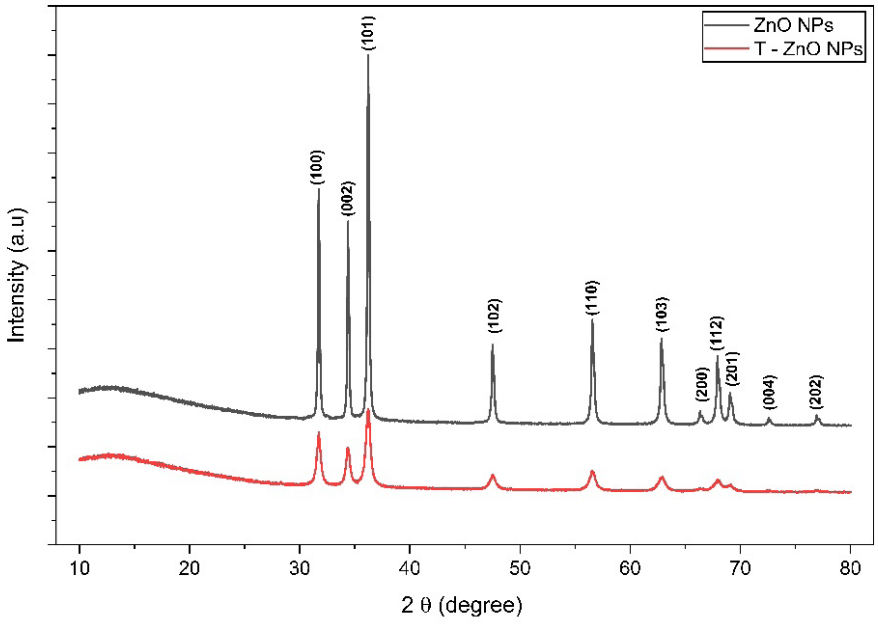


Fig. 4: XRD patterns of ZnO and T-ZnO NPs.

between 2850-2920cm^{-1}can be assigned to aliphatic C-H stretching vibrations. Crucially, the strong peaks in the region of 1600-1700 cm^{-1}correspond to C=O stretching of carbonyl/amide I or C=C stretching in aromatic rings. The band around 1380-1450 cm^{-1} can be related to C-H bending and carboxylate (-COO^{-}) vibrations in proteins. These phyto-biomolecules are evidently responsible for the reduction of zinc ions and the stabilization of the formed nanoparticles. However, the band around the 1200–1000 cm^{-1} region is mainly C-O/C-O-C stretching (polyphenols and sugars), indicating biomolecules capable of reducing and capping [38].

The FTIR spectra of both ZnO NPs and T-ZnO NPs show a significant simplification and a noticeable reduction in the intensity of these organic functional group peaks compared to the plant extract. This confirms the successful purification of the nanoparticles. The most prominent feature in both nanoparticle spectra is the strong, broad absorption band below 600 cm^{-1}, which is a definitive signature of the Zn-O stretching vibration mode, confirming the formation of the zinc oxide lattice [39].

The characteristic ZnO stretching vibration appears in the low-wavenumber region (~600-400 cm-1), confirming ZnO formation. With respect to the extract, the organic bands (O–H, C–H, C=O/C=C, C–O) appear weak and/or also somewhat displaced, which testifies to the adsorption of plant biomolecules on the ZnO surface as capping/stabilizing agents. 2 After thermal treatment, the organic-related bands (most significantly 2920–2850 cm -1 and 1700–1000 cm -1) decrease markedly in intensity, suggesting partial decomposition/removal of the plant peat-derived residues. After heating, the Zn-O band (~600-400 cm-1) is stronger/clearer, which suggests that the ZnO surface becomes cleaner and more inorganic after heating.

A critical observation is the sharper and more defined Zn-O peak in the T-ZnO NPs spectrum compared to the standard ZnO NPs. This indicates there exists a greater degree of crystallinity and more complete formation of the zinc-oxygen bonds in the treated structure. This is further supported by the almost total absence of residual organic peaks observed in the T-ZnO spectrum as opposed to residual shoulders still observed in the ZnO NPs spectrum , which suggests a more complete capping process and a purer overall inorganic crystal. Among several factors contributing to the enhanced T-ZnO NPs performance, in particular for photocatalytical purposes (where surface chemistry and charge carrier mobility are crucial), are this structural improvement of the T-ZnO NPs after the treatment, higher degree of crystallinity, more complete formation of zinc-oxygen bonds, and less defects/organic residues content on the surface of ZnO NPs [36].

Zeta potential measurements show ZnO NPs (38 mV) and hydrothermally treated T-ZnO NPs (46 mV), as illustrated in Fig. 6. The higher value of T-ZnO indicates enhanced surface charge and improved colloidal stability; this improvement in surface charge due to functionalization supports better dispersion behavior dominated by steric effects from the organic coating, consistent with recent findings that higher magnitude

J Water Environ Nanotechnol, 2026, 11(4): 522-534
10.22090/jwent.2026.2083327.2052

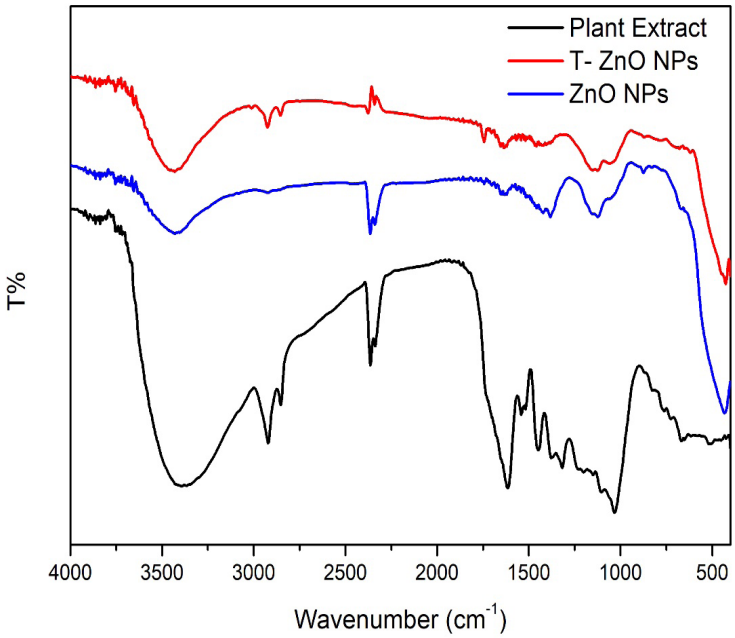


Fig. 5: FTIR of *Sesuvium portulacastrum* L.extract, ZnO NPs and T-ZnO NPs

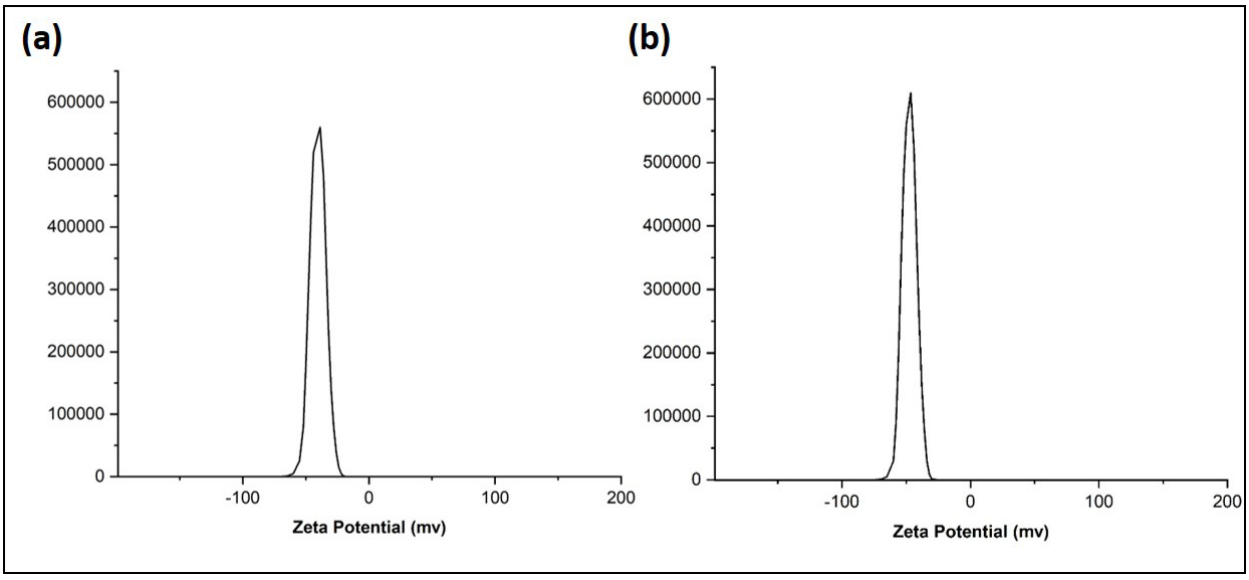


Fig. 6: Zeta potential (100 mg/L) of **(a)** ZnO NPs and **(b)**

zeta potentials correlate with stronger colloidal stability in ZnO systems [40].

T-ZnO NPs.

Thermogravimetric analysis (TGA) of pristine ZnO NPs and hydrothermally treated green-synthesized T-ZnO NPs shows three main weight-loss regions as shown in Fig. 7. The initial loss (≤150 °C) is ~3% for ZnO and ~6% for T-ZnO, due to desorbed water. In the 150–350 °C range, T-ZnO shows higher loss (~10%) than ZnO (~7%) from decomposition of surface-bound organics, confirming hydrothermal surface modification. At tempratures 350-700 °C, both lose 11%-12%, related to dehydroxylation and lattice changes. The lower residual mass of T-ZnO (73% vs. 78%) indicated higher thermally labile organic content [41].

The T-treatment process dramatically improved the photocatalytic performance of ZnO nanoparticles. They evidenced by superior kinetics and exceptional resilience under

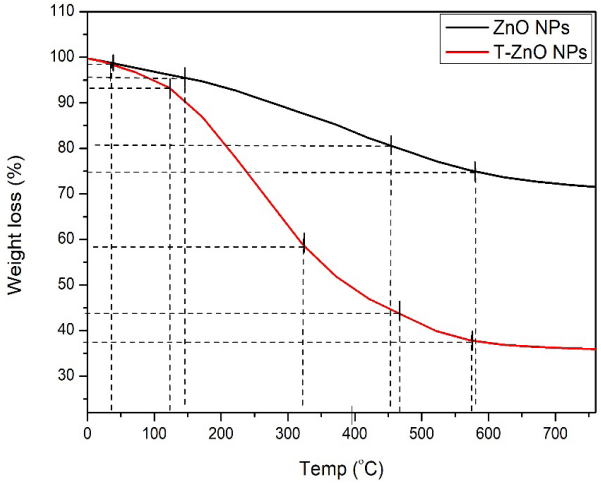


Fig. 7: TGA of ZnO NPs and T-ZnO NPs

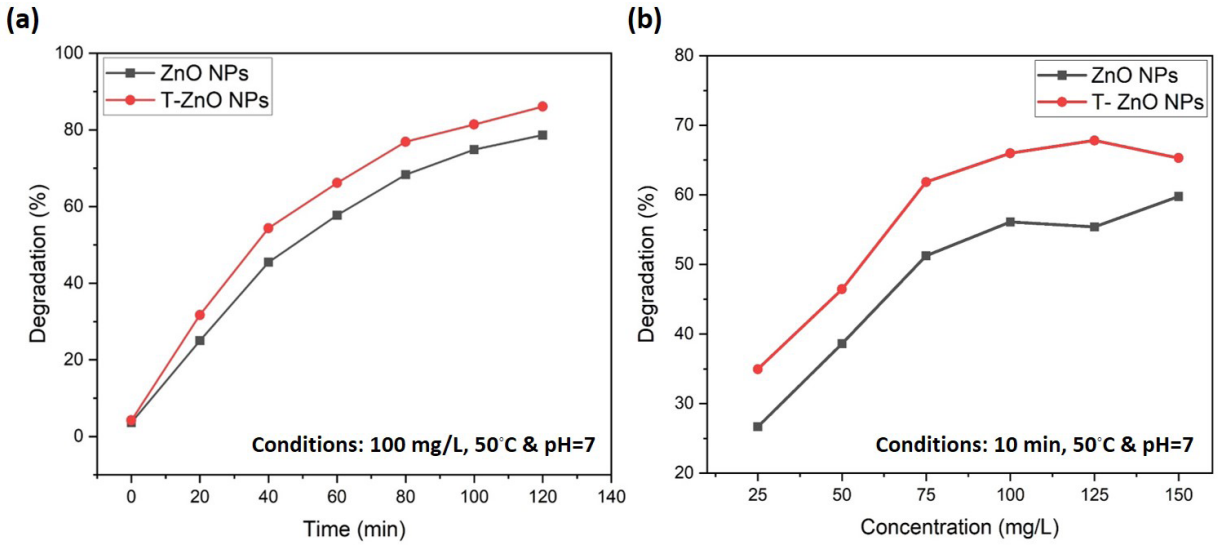


Fig. 8: (a) Photodegradation efficiency vs time & **(b)** Concentration Effect.

high pollutant load, as shown in Fig. 8. Also, Fig. 8a shows that T-ZnO NPs exhibited significantly accelerated kinetics, achieving 86% removal within 120 minutes. This is higher than the 78% obtained with pristine ZnO under the same conditions. Kinetic analysis confirmed an approximately 1.3-fold increase in the apparent rate constant (k), derived from the pseudo-first-order model according to the Arrhenius-type relation.

The increase in k value is attributable to the T-treatment engineering a higher density of surface oxygen vacancies. These defects act as efficient electron traps, drastically suppressing charge carrier recombination and boosting reactive oxygen species (ROS) generation [42]. However, this work surpassed recent reports on surface-modified ZnO systems, which typically showed just a 1.2- to 1.5-fold enhancement under comparable conditions.

Generally, this improvement is not merely kinetic. The concentration-dependent study (Fig. 8b) revealed that T-ZnO NPs achieved 68% degradation at 125 mg/L, compared to 55% for pristine ZnO under the same conditions. This showcases a robust catalytic capacity vital for real-world applications. This sustained result confirmed that the treatment creates a higher number of accessible active sites, overcoming the common limitation of site-shielding at high concentrations [43] [44].

Furthermore, T-ZnO nanoparticles (NPs) behave in a more favorable and stable manner under a wide range of environmental conditions like temperature and pH (Fig. 9). The photocatalytic activity of both catalysts increased with the reaction temperature in accordance with the Arrhenius law.

J Water Environ Nanotechnol, 2026, 11(4): 522-534
10.22090/jwent.2026.2083327.2052

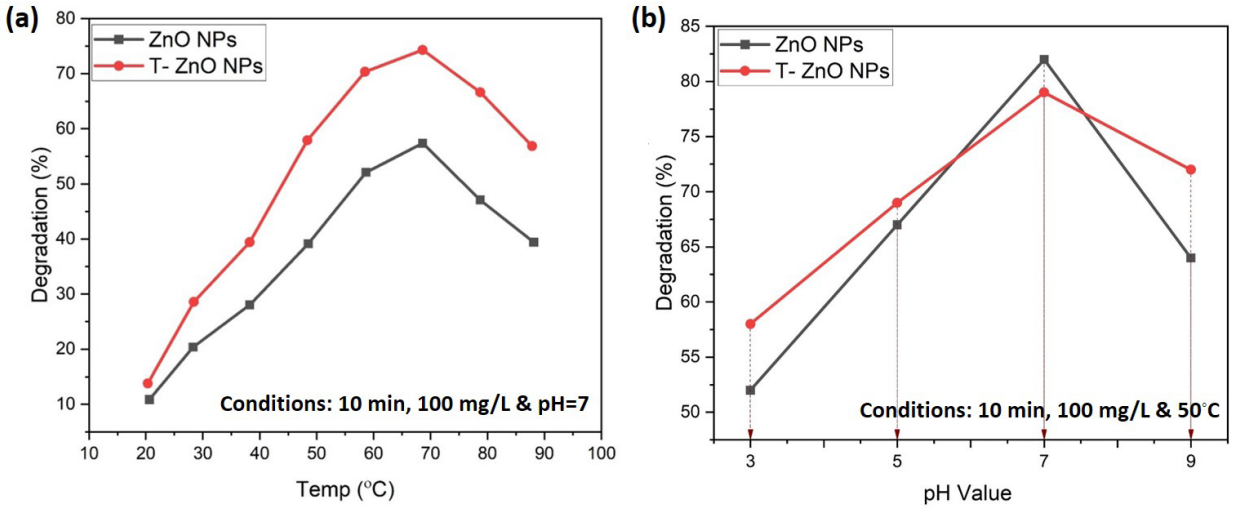


Fig. 9: (a) Effect of pH & **(b)** Temp. dependence on photocatalytic activity.

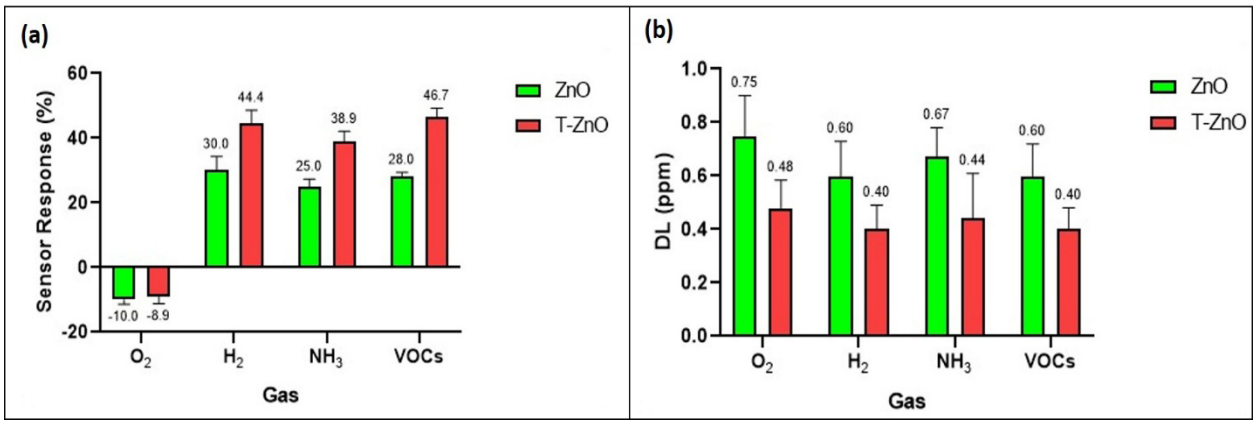


Fig. 10: Enhanced gas sensing performance of T-ZnO NPs compared to pristine ZnO NPs: **(a)** Sensor response (%) and **(b)** detection limit (ppm)

However, T-ZnO NPs exhibited superior efficiency over pristine ZnO NPs over all the temperature ranges studied, with the highest degradation efficiency of T-ZnO NPs being 69% at 70 °C, while that of ZnO was 57% at the same temperature, implying a ~1.2-fold catalytic enhancement between the two catalysts. The observed increase in thermal responsiveness indicates that T-treatment facilitates the accessibility of active sites and decreases the activation energy barrier to degradation, such that the rate of dye degradation is faster than that of ZnO alone, even at somewhat higher temperatures.

The T-ZnO catalyst also exhibited impressive pH stability (Fig. 9b). While the pristine ZnO showed pH-dependent changes in degradation, the treated catalyst maintained high efficiency under acidic, neutral, and basic pH conditions, with 82% degradation of the dye at pH = 7 compared with 78% for ZnO at the same pH, and optimal degradation was witnessed at pH = 9 in the case of T-ZnO. This pH-independent degradation stability is crucial for treating real wastewaters, where the pH is rarely constant. This suggests that the T-treatment passivates the surface against dissolution in acid and prevents unwanted aggregation in base, creating a more robust and versatile material. This broad pH operability significantly outperforms many recently reported modified photocatalysts that often show optimal activity only within a narrow pH window.

Although this phenomenon was mostly linked to the scattering, the comparative gas sensing characteristics indicated a substantial enhancement of T-ZnO NPs over pristine ZnO NPs, with the sensitivity factors markedly rising to the reducing gases such as H_2, NH_3, and volatile organic compounds (VOCs) (Fig. 10 a). Of these sensors, the best

response to detection of NH_3 and VOC was 46.7% and 50.0%, respectively. This increased susceptibility is presumably due to treatment regimen–induced conformation changes. Such synthesis could result in a higher amount of surface active sites and oxygen vacancies. Such defects are essential in tuning the surface depletion layer and facilitating the charge carrier transfer kinetics for surface redox reactions of analyte molecules with the sensor [45]. Additionally, this treatment probably increased the chemisorptions of ionic oxygen species (O_2^-, O^-) and thus stimulated the resistance change via the reaction between the electron donor reducing gases and ionic O species. The unusually high response to NH_3 and VOCs also indicates a customized surface chemistry that preferentially promotes interaction with nitrogenous (acid/base) and organic compounds, presumably via either acid-base interactions or improved catalytic decomposition.

Analysis of DL revealed that the treated ZnO nanoparticles (T-ZnO NPs) exhibited a superior sensing performance towards all the analytes (Fig. 10 b). Compared with untreated ZnO NPs, the T-ZnO NP sensor demonstrated significantly lower detection limits, achieving H_2 and VOCs detection limits of 0.4 ppm, which were reduced from 0.6 ppm and 0.67 ppm for ZnO NPs, respectively. It affirms that this treatment protocol improves the capability of the sensor to detect respective gases at the lowest concentrations across the board. This improvement in the detection limit is a result of the increase in surface reactivity and electronic sensitisation resulting from the treatment. Lower DL means fewer gas molecules are needed to cause a significant and reproducible change in electrical resistance. At the core level, this depends on the interaction strength between the analyte molecule and the sensor surface. This increase in density of oxygen vacancies through the treatment can decrease the activation energy for the surface reaction, facilitating a higher degree of electronic perturbation even at the ultra-low gas concentrations. In addition, the T-ZnO NPs increased the signal-to-noise ratio (SNR), also making the weak signal from a low number of target molecules distinguishable from the resting electrical noise of the device [35] [17]. The superior DL for H_2 and VOCs (0.4 ppm) aligns with the highest sensor responses observed for these analytes in Fig. 10a**,** suggesting a particularly favorable chemisorption process on the modified T-ZnO surface.

Hydrothermal T-treatment greatly improves the photocatalytic and sensing performance of green-synthesized ZnO Nanoparticles. Optimised conditions (i.e., 30 min irradiation time, 125 mg/L pollutant concentration, pH = 9 and 70 °C) led to 86% degradation with T-ZnO NPs superior to pristine ZnO (78%) and a reduction in reaction rate constant by a factor of ~1.3 due to higher density of oxygen vacancy, facilitated charge separation, and enhanced ROS generation for T-ZnO NPs. T-ZnO NPs were very effective and stable in a wide range of temperatures and pH, so the high efficiencies achieved by T-ZnO NPs under acidic, neutral, and alkaline conditions indicated their excellent robustness for practical wastewater treatment. In addition, gas sensing performance, including responsiveness of 46.7% to NH_3 and 50% to VOCs, and ultra-low detection limits in the order of 0.4 ppm, were significantly enhanced and attributed to the improved surface activity and electronic sensitization.

CONCLUSION

This study showed the feasibility of green and low-cost synthesis of ZnO nanoparticles with well-defined morphology using leaf extract of *Sesuvium portulacastrum L.*, although further hydrothermal treatment could greatly improve their properties. The improved crystallinity, narrower band gap, lower impurity adsorption, and increased density of defect sites drastically enhance the catalytic and functional performances of the T-ZnO NPs. T-ZnO NPs assembled of numerous crystalline arrays have been found to degrade organic pollutants more quickly and effectively, as well as to show improved gas sensing behavior with increased response and decreased detection limits to reducing gases compared to pristine ZnO. Such encouraging results reveal the high potential of the combined plant-mediated synthesis and hydrothermal modification approach as a green and sustainable approach for designing multifunctional ZnO nanomaterials for environmental remediation and sensing applications. Next studies may concentrate on developing the appropriate treatment parameters, understanding how the defects form, and incorporating the material into devices.

Author's Contributions

Study Conception or Design: Mawlood Maajal Ali, Rafaa Abd Alkareem Abdulwahid,
Data Acquisition: Hadeel Salih Mahdi, Rafaa Abd Alkareem Abdulwahid,
Data Analysis or Interpretation: Mawlood Maajal Ali, Hadeel Salih Mahdi, Mustafa Nadhim Owaid
Manuscript Drafting: Mawlood Maajal Ali, Mustafa Nadhim Owaid
Critical Manuscript Revision: Mustafa Nadhim Owaid, Mawlood Maajal Ali
All authors have approved the final manuscript and are responsible for all aspects of the work.

Funding

This research received no external funding.

Acknowledgments:

The authors wish to thank the University of Anbar (www.uoanbar.edu.iq) for all of its support. We would like to thank the outstanding academic staff of the University of Anbar for their encouragement and for providing the technical, scientific, and research-related resources necessary to complete this research.

Conflict of interest:

There are no conflicts of interest in this study

REFERENCES

1. Swain M, Mishra D, Sahoo G (2025) A review on green synthesis of ZnO nanoparticles. Discov Appl Sci 7:997
2. Thakur N, Tapwal A, Kumari K, et al (2025) Advancements in biogenic nanoparticles synthesis, characterization and its mechanism in disease management. Bioresour Technol Rep 31:102227. https://doi.org/10.1016/j.biteb.2025.102227
3. Ibrahem KH (2025) Green Synthesis of Nanoparticles Using Plants:(Article Review). Journal of Kirkuk University for Agricultural Sciences 16:72–78
4. Abdelbaky AS, Abd El-Mageed TA, Babalghith AO, et al (2022) Green synthesis and characterization of ZnO nanoparticles using Pelargonium odoratissimum (L.) aqueous leaf extract and their antioxidant, antibacterial and anti-inflammatory activities. Antioxidants 11:1444. https://doi.org/10.3390/antiox11081444
5. Sarwar K, Nazli ZI, Munir H, et al (2025) Biosynthesis of zinc oxide nanoparticles using Moringa oleifera leaf extract, probing antibacterial and antioxidant activities. Sci Rep 15:20413. https://doi.org/10.1038/s41598-025-08839-w
6. Hossain E, Lee JS, Kwon KS (2025) Photocatalytic Degradation of Hydrothermally Grown Zinc Oxide Nanorods on a Silver Seed Layer. ACS Omega 10:5708–5721. https://doi.org/10.1021/acsomega.4c09121
7. Zango ZU, Garba A, Shittu FB, et al (2025) A state-of-the-art review on green synthesis and modifications of ZnO nanoparticles for organic pollutants decomposition and CO2 conversion. Journal of Hazardous Materials Advances 17:100588. https://doi.org/10.1016/j.hazadv.2024.100588
8. Mousa SA, Wissa DA, Hassan HH, et al (2024) Enhanced photocatalytic activity of green synthesized zinc oxide nanoparticles using low-cost plant extracts. Sci Rep 14:16713. https://doi.org/10.1038/s41598-024-66975-1
9. Mohamed KM, Benitto JJ, Vijaya JJ, Bououdina M (2023) Recent advances in ZnO-based nanostructures for the photocatalytic degradation of hazardous, non-biodegradable medicines. Crystals (Basel) 13:329
10. Mustapha N, Ben Abdelaziz B, Benamara M, Hjiri M (2025) Recent Advances in Doping and Polymer Hybridization Strategies for Enhancing ZnO-Based Gas Sensors. Nanomaterials 15:1609. https://doi.org/10.3390/nano15211609
11. Zhu C, Wang X (2025) Nanomaterial ZnO synthesis and its photocatalytic applications: A review. Nanomaterials 15:682
12. Taha I, Abdulhamid ZM, Straubinger R, et al (2024) Ga-doped ZnO nanoparticles for enhanced CO2 gas sensing applications. Sci Rep 14:29712
13. Mahajan M, Kumar S, Gaur J, et al (2025) Green synthesis of ZnO nanoparticles using Justicia adhatoda for photocatalytic degradation of malachite green and reduction of 4-nitrophenol. RSC Adv 15:2958–2980. https://doi.org/10.1039/d4ra08632e
14. Ali MM, Abbas JA, Owaid MN, Zaidan TA (2025) Effect of hydrothermal treatment on optical properties of gold nanoparticles synthesized from Lepidium sativum seeds and their applications. Current Applied Physics 80:383–391. https://doi.org/10.1016/j.cap.2025.10.011
15. Bani-Atta SA, Darwish AAA, Shwashreh L, et al (2024) Efficient Photocatalytic Degradation of Methylene Blue and Methyl Orange Using Calcium-Polyoxometalate Under Ultraviolet Irradiation. Processes 12:. https://doi.org/10.3390/pr12122769
16. Liang P, Yang W, Peng H, Zhao S (2024) Efficient Degradation of Methylene Blue in Industrial Wastewater and High Cycling Stability of Nano ZnO. Molecules 29:. https://doi.org/10.3390/molecules29235584
17. Franco MA, Conti PP, Andre RS, Correa DS (2022) A review on chemiresistive ZnO gas sensors. Sensors and Actuators Reports 4:. https://doi.org/10.1016/j.snr.2022.100100
18. Parys W, Pyka-Pająk A (2022) Influence of Chromatographic Conditions on LOD and LOQ of Fluoxetine and Sertraline Analyzed by TLC-Densitometric Method. Processes 10:. https://doi.org/10.3390/pr10050971
19. Al-Wadi AM, Al-Mammar DE (2022) Green Synthesis by Zygophyllum Coccineum Leaves Extract for Preparing ZnO Nanoparticles, and Characteristics Study. Egypt J Chem 65:363–369
20. Batterjee MG, Nabi A, Kamli MR, et al (2022) Green hydrothermal synthesis of zinc oxide nanoparticles for UV-light-induced photocatalytic degradation of ciprofloxacin antibiotic in an aqueous environment. Catalysts 12:1347
21. Özgür Ü, Alivov Y, Liu C, et al (2005) A comprehensive review of ZnO materials and devices. J Appl Phys 98:041301. https://doi.org/10.1063/1.1992666
22. Sirelkhatim A, Mahmud S, Seeni A, et al (2015) Review on zinc oxide nanoparticles: Antibacterial activity and toxicity mechanism. Nanomicro Lett. 7:219–242
23. Javed R, Zia M, Naz S, et al (2020) Role of capping agents in the application of nanoparticles in biomedicine and environmental remediation: recent trends and future prospects. J. Nanobiotechnology 18
24. Yang J, Liu X, Yang L, et al (2009) Effect of annealing temperature on the structure and optical properties of ZnO nanoparticles. J Alloys Compd 477:632–635. https://doi.org/10.1016/j.jallcom.2008.10.135
25. Elumalai K, Velmurugan S (2015) Green synthesis, characterization and antimicrobial activities of zinc oxide nanoparticles from the leaf extract of Azadirachta indica (L.). Appl Surf Sci 345:329–336. https://doi.org/10.1016/j.apsusc.2015.03.176
26. Yao S, Li Y, Xue L, Yan Y (2010) Photoluminescence properties of Ba2ZnSi2O7:Eu2+, Re3+ (Re = Dy, Nd) long lasting phosphors prepared by the combustion-assisted synthesis method. J Alloys Compd 490:200–203. https://doi.org/10.1016/j.jallcom.2009.09.025
27. Srikant V, Clarke DR (1998) On the optical band gap of zinc oxide. J Appl Phys 83:5447–5451
28. Warkad IR, Paul R, Parthiban S, Gawande MB (2024) Highly selective oxidation of biomass-derived alcohols and aromatic alcohols to aldehydes over Ti3C2-TiO2 nanocomposites under visible light. J Environ Chem Eng 12:113128
29. Chitra M, Mangamma G, Uthayarani K, et al (2020) Band gap engineering in ZnO based nanocomposites. Physica E Low Dimens Syst Nanostruct 119:113969
30. Ferlazzo A, Neri G, Donato A, et al (2025) Room Temperature NO2-Sensing Properties of N-Doped ZnO Nanoparticles Activated by UV-Vis Light. Sensors 25:. https://doi.org/10.3390/s25010114
31. Nath RA, Raj A, Salam JA, et al (2023) Self-powered photodetector based on copper-doped methyl ammonium lead bromide. Journal of Materials Science: Materials in Electronics 34:1086

32. Huang Y, Pan Y, Huang X, et al (2023) Porous NiS@ Ni2P nanoframe as a multi-functional catalyst for enhanced oxygen evolution and urea oxidation reactions. Journal of Industrial and Engineering Chemistry 118:239–246
33. Vayssieres L (2003) Growth of arrayed nanorods and nanowires of ZnO from aqueous solutions. Advanced Materials 15:464–466. https://doi.org/10.1002/adma.200390108
34. Thiam M, Bernardo ADJ, Pellegrini VDOA, et al (2025) Green Synthesis of ZnO Nanoparticles Using Licania tomentosa Benth (Oiti) Leaf Extract: Characterization and Applications for the Photocatalytic Degradation of Crystal Violet Dye. Processes 13:880
35. Wang ZL (2004) Zinc oxide nanostructures: growth, properties and applications. Journal of physics: Condensed Matter 16:R829
36. Mishra YK, Adelung R (2018) ZnO tetrapod materials for functional applications. Materials Today 21:631–651
37. Coates J (2000) Interpretation of infrared spectra, a practical approach. Encyclopedia of Analytical Chemistry 12:10815–10837
38. Li AP, Peng H, Peng JD, et al (2015) Rayleigh light scattering detection of three α1-adrenoceptor antagonists coupled with high performance liquid chromatograph. Spectrochim Acta A Mol Biomol Spectrosc 147:178–184. https://doi.org/10.1016/j.saa.2015.02.062
39. Kołodziejczak-Radzimska A, Jesionowski T (2014) Zinc oxide—from synthesis to application: a review. Materials 7:2833–2881
40. José BJA, Shinde MD (2024) Colloidal stability and dielectric behavior of eco-friendly synthesized zinc oxide nanostructures from Moringa seeds. Sci Rep 14:2310
41. Negi A, Ringwal S, Pandey M (2024) Plant-mediated Z-scheme ZnO/TiO2-NCs for antibacterial potential and dye degradation: experimental and DFT study. Sci Rep 14:7955
42. Li H, Li J, Ai Z, et al (2018) Oxygen vacancy-mediated photocatalysis of BiOCl: reactivity, selectivity, and perspectives. Angewandte Chemie International Edition 57:122–138. https://doi.org/10.1002/anie.201705628
43. Premalatha N, Rex P (2024) A comprehensive review on photocatalytic degradation of organophosphorus pesticide using ZnO coupled photocatalysts. Desalination Water Treat 320:100753. https://doi.org/10.1016/j.dwt.2024.100753
44. Fang G, Wang J, Yang Q, et al (2023) Highly-efficient cathodic lysis of biofilm on conductive carbon nanotube membranes. Sep Purif Technol 304:122327. https://doi.org/10.1016/j.seppur.2022.122327
45. Rani N, Sagar NA, Chauhan A, Mondal A (2025) Green synthesis of ZnO nanoparticles: Characterization and emerging applications in sustainable agriculture. Ind Crops Prod 233:121393. https://doi.org/10.1016/j.indcrop.2025.121393